IJMMM International Journal of Minerals, Metallurgy and Materials 矿物冶金与材料学报（英文版）

Evaluation of the microstructure, thermal and mechanical properties of Cu/SiC nanocomposites fabricated by mechanical alloying

Essam B. Moustafa and Mohammed A. Taha

Cite this article as:
Essam B. Moustafa and Mohammed A. Taha, Evaluation of the microstructure, thermal and mechanical properties of Cu/SiC nanocomposites fabricated by mechanical alloying, *Int. J. Miner. Metall. Mater.*, 28(2021), No. 3, pp. 475-486. https://doi.org/10.1007/s12613-020-2176-z

---

International Journal of Minerals, Metallurgy and Materials
Volume 28, Number 3, March 2021, Page 475
https://doi.org/10.1007/s12613-020-2176-z

Evaluation of the microstructure, thermal and mechanical properties of Cu/SiC nanocomposites fabricated by mechanical alloying

Essam B. Moustafa[1)] *and Mohammed A. Taha*[2)]

1) Mechanical Engineering Departments, Faculty of Engineering, King Abdulaziz University, Jeddah 21589, Saudi Arabia
2) Solid State Physics Department, National Research Centre, El Buhouth St., Dokki, 12622 Giza, Egypt
(Received: 11 June 2020; revised: 24 August 2020; accepted: 25 August 2020)

Abstract: Nano-sized silicon carbide (SiC: 0wt%, 1wt%, 2wt%, 4wt%, and 8wt%) reinforced copper (Cu) matrix nanocomposites were manufactured, pressed, and sintered at 775 and 875°C in an argon atmosphere. X-ray diffraction (XRD) and scanning electron microscopy were performed to characterize the microstructural evolution. The density, thermal expansion, mechanical, and electrical properties were studied. XRD analyses showed that with increasing SiC content, the microstrain and dislocation density increased, while the crystal size decreased. The coefficient of thermal expansion (CTE) of the nanocomposites was less than that of the Cu matrix. The improvement in the CTE with increasing sintering temperature may be because of densification of the microstructure. Moreover, the mechanical properties of these nanocomposites showed noticeable enhancements with the addition of SiC and sintering temperatures, where the microhardness and apparent strengthening efficiency of nanocomposites containing 8wt% SiC and sintered at 875°C were 958.7 MPa and 1.07 vol%$^{-1}$, respectively. The electrical conductivity of the sample slightly decreased with additional SiC and increased with sintering temperature. The prepared Cu/SiC nanocomposites possessed good electrical conductivity, high thermal stability, and excellent mechanical properties.

Keywords: copper matrix nanocomposites; silicon carbide; coefficient of thermal expansion; elastic moduli; electrical conductivity; mechanical alloying

1. Introduction

Owing to good chemical stability and excellent thermal and electrical conductivities, great effort has been directed towards copper (Cu) and its alloys for use in different engineering applications. Unfortunately, the mechanical properties of Cu and its alloys are low, particularly at high temperatures, and consequently, their applications are limited. Therefore, fabricating Cu matrix composites by producing secondary phases in Cu and its alloys is considered an optimum solution [1−2]. In this regard, the enhancement in the mechanical properties of Cu, such as hardness, compressive strength, and Young's modulus, is strongly correlated to the reinforcement type, the particle size, and the distribution [3−5]. Sorkhe *et al*. [3] fabricated Cu–TiO_2 composites with various percentages of TiO_2 (0wt%, 1wt%, 3wt%, 5wt%, and 7wt%) through a mechanical alloying method to investigate the density, mechanical, and electrical properties of the composites. The microhardness of the nanocomposites was increased to approximately HV 100, while the electrical conductivity decreased by approximately 110% with increasing TiO_2 up to 7wt%. Taha and Zawrah [4] investigated the effect of different ZrO_2 contents (up to 12wt%) on the mechanical properties and electrical conductivity of a Cu matrix. They observed a remarkable improvement in the strength of the Cu matrix with a noticeable effect on the electrical conductivity. Akbarpour *et al*. [5] investigated the influence of variously sized silicon carbide (SiC) particles on the morphology, strength, and wear behavior of a Cu matrix. The results showed that the nanocomposite had higher wear resistance and improved strength compared with the microcomposite. Based on this effort, nano-SiC is considered one of the best additives for Cu because of its superior mechanical properties, perfect thermal conductivity, low density, low coefficient of thermal expansion (CTE), and good electrical conductivity [6−7]. Additionally, a handful of researchers have worked on improving the mechanical properties of aluminum [6], magnesium [8], and Cu [5] with SiC. However, these works are hindered by the lack of proper distribution of SiC into the matrix of composite systems [7−9]. Amazingly, most

Corresponding author: Mohammed A. Taha E-mail: mtahanrc@gmail.com

composites based on metal suffer from CTE mismatch of two joining materials, which consequently contributes to producing stress and strain at the joining interface. These consequences are considered serious because they negatively affect the properties of the composites [10]. Notably, several studies discussed the effect of different ceramic types, i.e., SiC [10], lead titanate ($PbTiO_3$) [11], and tungsten carbide (WC) [12], on the thermal properties of the Cu matrix.

Generally, there are two routes for synthesizing reinforced nanocomposites based on Cu. One route deals with using chemical reactions/phase transformations with the aim of the *in-situ* formation of reinforcement particles in Cu-based nanocomposites [13]. The second route uses mechanical alloying or selective fracturing of secondary particles via a mechanical approach to disperse the reinforcements into the matrix [14−15]. Since mechanical alloying is a suitable and cost-effective process, it is broadly utilized to prepare many nanocomposites [16−17]. It is important to note that the latter route relies on several factors, including time, speed, ball-to-powder ratio (BPR), atmosphere, temperature, and the reinforcement type [18−19]. Based on the abovementioned considerations, the major objective of this article is to produce Cu matrix nanocomposites with different weight percentages of nano-sized SiC (up to 8wt%) and sintered at 875°C to obtain nanocomposites with better densification. Additionally, the properties, including microhardness, elastic moduli, and apparent strengthening efficiency of the nanocomposites were extensively studied. The microstructure, thermal expansion, physical, and electrical properties were also studied.

2. Experimental

In order to produce Cu matrix nanocomposite powders with various SiC contents, i.e., 0wt%, 1wt%, 2wt%, 4wt%, and 8wt%, using the mechanical alloying method, pure Cu and SiC (99.9% purity; particle sizes of 200 nm and 55 nm, respectively) were used as starting materials. A planetary ball mill with Al_2O_3 containers and balls was employed using the following conditions of milling time, speed, and BPR of 20 h, 550 r/min, and 20:1, respectively. Transmission electron microscopy (TEM) was used to investigate the microstructure of as-received Cu and nano-SiC particles as shown in Fig. 1. The mean particle size of Cu was approximately 203 nm and particles exhibited high agglomeration, while the SiC particles were approximately 39 nm with low agglomeration.

The phase compositions of the milled powders were investigated by X-ray diffraction (XRD) analysis. The crystalline size (C), lattice strain (ε), and dislocation density (δ) were determined from the X-ray line broadening (B) for the principle (hkl) planes, i.e., (111), (200), (220), and (311) at 2θ = 43.317°, 50.499°, 74.126°, and 89.938°, respectively, using the equations mentioned in Refs. [20−21]:

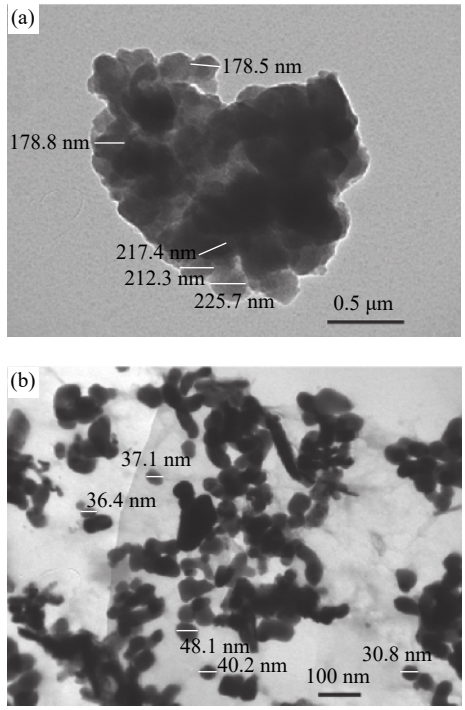

Fig. 1. TEM micrographs of as-received (a) Cu and (b) SiC particles.

$$C = \frac{0.9\lambda}{B\cos\theta} \quad (1)$$

$$\varepsilon = \frac{B}{4\tan\theta} \quad (2)$$

$$\delta = \frac{1}{C^2} \quad (3)$$

where the wave length λ = 0.1540591 nm (Cu–Ni radiation) and θ is the diffraction angle in rad. Subsequently, the resultant powders were cold pressed to pellets and sintered at 775 and 875°C for 1 h in argon with a heating rate of 5°C/min. The physical properties of the fired samples were measured using the Archimedes method (ASTM: B962-13). Moreover, the theoretical density of the samples was calculated by the mixture rule, and consequently the relative density was calculated. Microstructures of the powder and sintered samples were examined by scanning electron microscopy (SEM, Quanta FEG25). Thermal expansion measurements of the sintered nanocomposite samples were studied from 50 to 600°C in air. The microhardness of the nanocomposites was evaluated by a Vickers tester (Vickers hardness machine-model: Shimadzu corporation hardness tester) [22].

The longitudinal (V_L) and shear ultrasonic velocities (V_S) were measured using the pulse-echo technique.

Alternatively, the constants of Lame (i.e., β and μ) were calculated according to the formulas in Refs. [23−24]:

$$\beta = \rho(V_L^2 - 2V_S^2) \quad (4)$$

$$\mu = \rho V_S^2 \quad (5)$$

where ρ is the bulk density.

The elastic modulus (L), Young's modulus (E), shear modulus (G), bulk modulus (K), and Poisson's ratio (υ) of the nanocomposites were calculated by the following equations [24–25]:

$$L = \beta + 2\mu \quad (6)$$

$$G = \mu \quad (7)$$

$$E = \mu\frac{3\beta + 2\mu}{\beta + \mu} \quad (8)$$

$$K = \beta + \frac{2}{3}\mu \quad (9)$$

$$\upsilon = \frac{\beta}{2(\beta + \mu)} \quad (10)$$

The compressive tests of the specimens were studied using ASTM standard E9. Furthermore, the yield strength, ultimate strength elongation, and apparent strengthening efficiency were calculated from the stress–strain curve. The electrical conductivity of the nanocomposites was measured using a Keithley 6517B system according to the formula in Ref. [2]. All preparation and characterization steps are illustrated in Fig. 2.

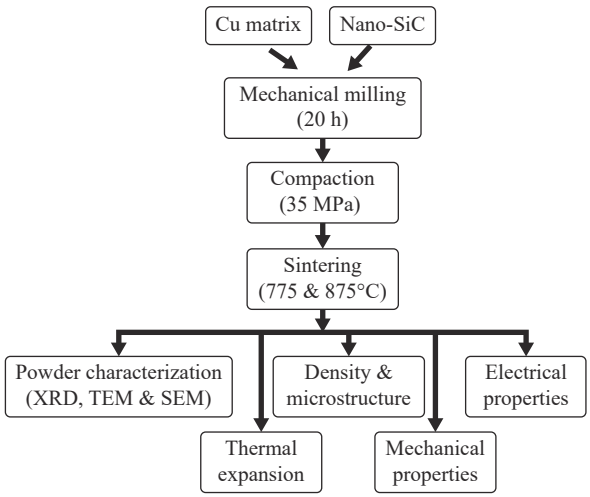

Fig. 2. Schematic of the production and characterization of nanocomposites.

3. Results and discussion

3.1. Properties of the nanocomposites powders

3.1.1. X-ray diffraction

Fig. 3 displays the XRD patterns of Cu/SiC nanocomposite powders with different SiC contents (i.e., 0wt%, 1wt%, 2wt%, 4wt%, and 8wt%) after 20 h of milling. The XRD patterns were analyzed according to JCPDS 85-1362 and 89-2225 standard cards. The patterns were mainly composed of Cu and SiC phases (primary phases of the starting mixture) considering that Cu and SiC powders exhibit cubic and rhombohedral crystal structures, respectively. Importantly, the absence of the characteristic SiC peaks in the nanocomposites with 1wt% and 2wt% SiC is attributed to the low weight percentages of SiC, which are below the XRD detection limit. After the milling process, a significant broadening with a decrease in the intensity of peaks of the Cu matrix occurred while the intensity of the SiC peaks increased with increasing weight percentage of the nano-SiC particles [26].

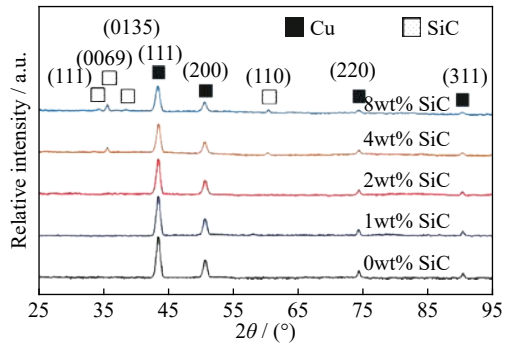

Fig. 3. XRD patterns of nanocomposite powders with different SiC contents.

In order to characterize the microstructure of the prepared nanopowders, the Cu matrix crystallite size, dislocation density, and microstrain of the Cu/SiC nanocomposite powders after 20 h of milling were calculated using the broadening of their diffraction peaks. The effects of the SiC content on the crystallite size, dislocation density, and microstrain of the Cu/SiC nanocomposite powders are illustrated in Fig. 4. Notably, with the increase in SiC weight percentage, the crystal size decreased while the dislocation density and microstrain increased because of severe plastic deformation and grain size refinement during mechanical alloying process due to the added nano-SiC particles [6,27]. The crystal sizes of Cu–0wt%, 1wt%, 2wt%, 4wt%, and 8wt% SiC milled powders were 21.03, 20.69, 19.95, 18.1, and 14.33 nm, while the microstrains were 0.3333%, 0.3383%, 0.3522%, 0.3857%, and 0.4915%, respectively.

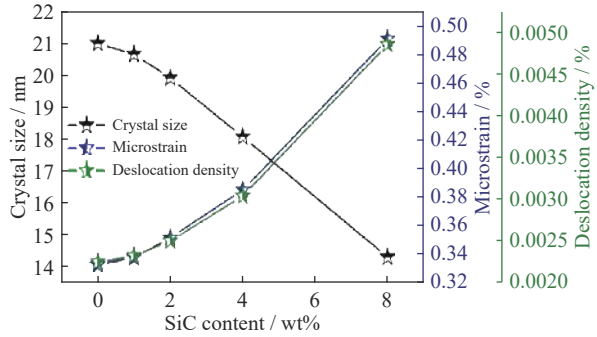

Fig. 4. Crystal sizes, lattice strains (microstrains), and dislocation densities of nanocomposite powders as a function of the SiC content.

3.1.2. SEM analyses

Generally, the existence of metal (ductile) particles in ceramics (brittle) forms a ductile–brittle system, which leads

to several changes during the milling process. First, the ductile particles suffer from deformation, while brittle particles suffer from fragmentation. Based on this behavior, brittle particles tend to stay between ductile particles at the instant of ball collision [5,19,28]. As a result, a real composite is formed. The morphology of the Cu matrix and Cu/SiC nanocomposite powders were investigated using SEM as shown in Fig. 5. With the increase in nano-SiC reinforced particles, a finer nanocomposite powder was obtained with homogenous distribution of SiC particles in the Cu matrix, which was substantial for improving the mechanical, electrical, and thermal properties. Surprisingly, SEM images are an insufficient method to ensure uniform distribution of SiC particles into Cu matrix because of the incorporation of SiC particles into grain boundaries of Cu. Therefore, chemical element distribution maps of samples containing 4wt% and 8wt% SiC were obtained as shown in Figs. 6(a) and 6(b).

3.2. Properties of the sintered nanocomposite samples

3.2.1. Physical properties

To obtain Cu/SiC nanocomposites with high densification, their powders were compacted and sintered. During the sintering process, the necks at the boundaries between the particles grew, which produced the sintered nanocomposites at the desired densification. Theoretical, bulk, and relative densities and the apparent porosities of the nanocomposite samples sintered for 1 h at 775 and 875°C with various SiC contents are shown in Table 1. The relative densities of the specimens were remarkably reduced with an increase in the weight percentage of the SiC reinforced particles. Alternatively, the apparent porosity increased by the same factor.

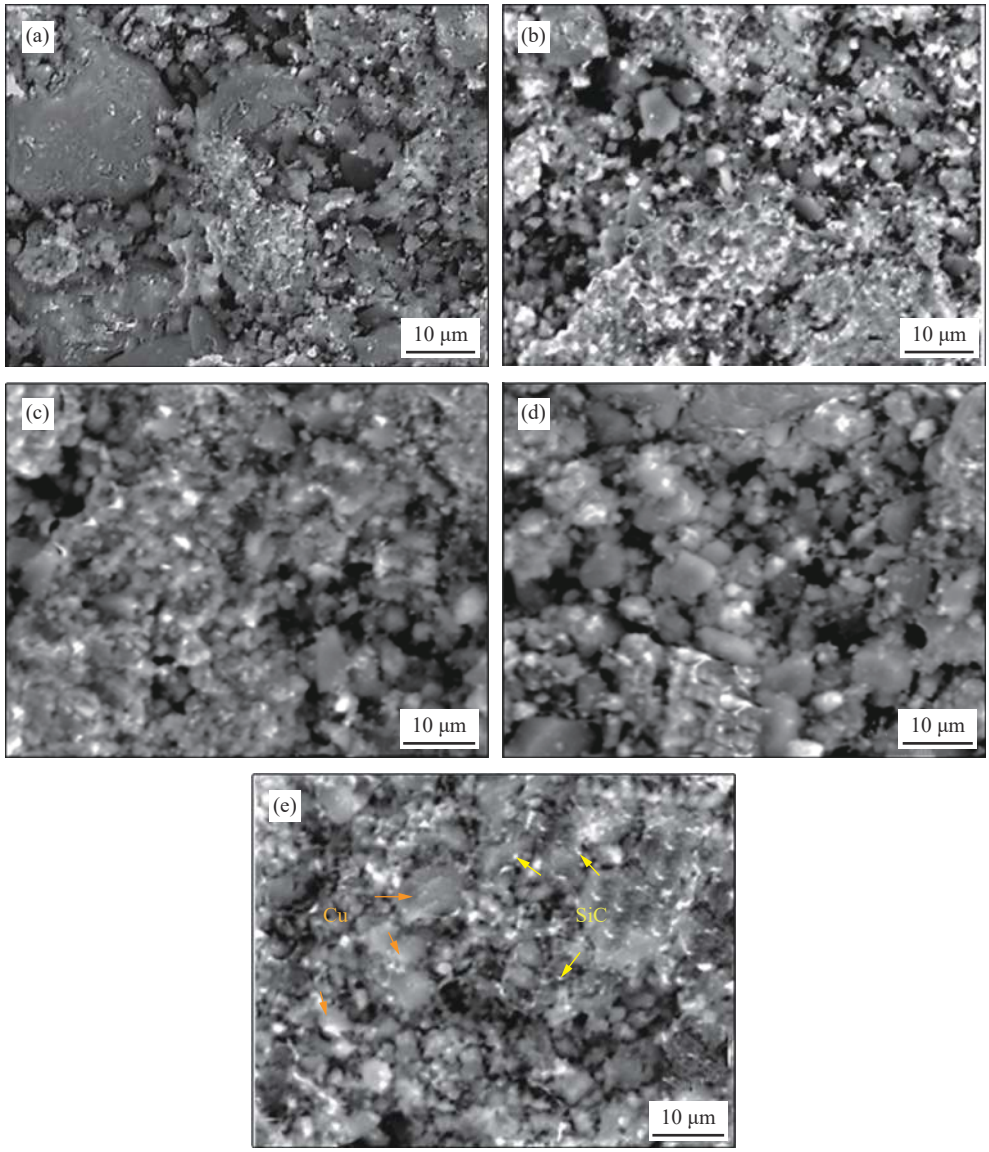

Fig. 5. SEM images of (a) Cu–0wt%SiC, (b) Cu–1wt%SiC, (c) Cu–2wt%SiC, (d) Cu–4wt%SiC, and (e) Cu–8wt%SiC milled powder specimens.

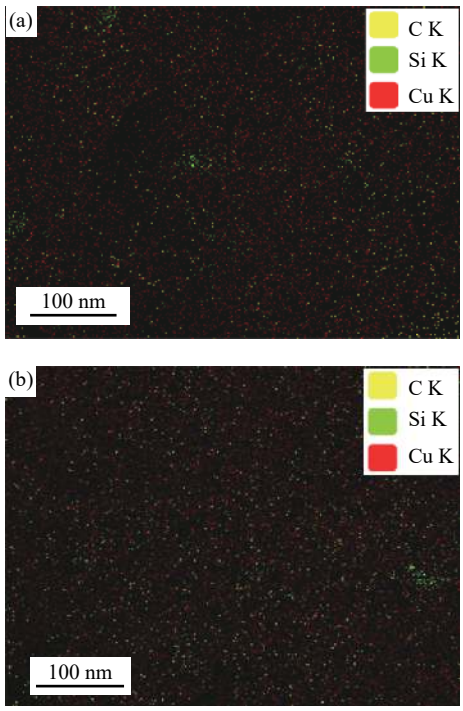

Fig. 6. SEM/energy dispersive spectroscopy (EDS) maps of the surface distributions of elements for Cu/SiC composite powders containing (a) 4wt% SiC and (b) 8wt% SiC.

With increasing sintering temperature from 775 to 875°C, the relative densities of the specimens increased, while the apparent porosity decreased. The major reason behind this behavior is the presence of SiC, which has lower compressibility than that of the Cu matrix and a large difference in the melting temperatures (Cu: ~1080°C; SiC: ~2730°C), which leads to weak bonding and subsequently limits diffusion. Furthermore, the SiC reinforcement particles act as a barrier during the diffusion step of sintering process [29–30]. Similarly, increased amounts of ceramic particles (i.e., ZrO_2, SiC, and TiC particles) in the Cu matrix reduce the relative density of the sintered nanocomposites [4–6,31]. Generally, the ceramics are responsible for low diffusion at the interface between the matrix and reinforcement; therefore, the densification of the sintered nanocomposites decreases [29,32]. The measurable improvement in the density, i.e., reduced porosity with increasing sintering temperature to 875°C, may be because of the increasing diffusion rate that contributes to increase the contacts between particles, grain growth, and decreasing the pore volume [33–34]. Hence, higher relative densities (lower porosity) were achieved at higher sintering temperature. This trend can be more clarified using Eq. (11), which shows that the sintering temperature plays an essential role in the diffusion process [35]:

$$D = D_0 e^{\frac{-Q}{RT}} \tag{11}$$

where D, D_0, Q, R, and T are the diffusion coefficient, constant, activation energy, Boltzmann's constant, and temperature, respectively.

3.2.2. Microstructure

SEM micrographs of the nanocomposite specimens with 2wt% and 8wt% SiC sintered at 775 and 875°C are shown in Figs. 7 and 8. An increase in nano-SiC particles contributed to an observable change in the microstructure of the nanocomposites, which led to an increase in porosity and considerable weakness in the contact between Cu particles. As shown in Fig. 7, the bonding between SiC and Cu was weak because of the insufficient sintering temperature. However, by increasing the sintering temperature to 875°C, a suitable bonding strength between SiC and Cu was reached (Fig. 8). The sintering temperature is responsible for better densification behavior, as shown by the grain growth and decrease in the number of pores [36].

3.2.3. Thermal expansion

Fig. 9 illustrates the relative expansion versus temperature of Cu/SiC nanocomposites with various weight percentages of nano-SiC particles. Generally, the relative expansion (dl/l_0) of the nanocomposites with various SiC contents increased as the temperature increased significantly. Furthermore, it reduced with increasing SiC weight percentage. The CTE values of samples with different sintering temperatures are shown in Fig. 10. The CTE value decreased with increased SiC content and increased with increasing sintering temper-

Table 1. Theoretical, bulk, and relative densities and apparent porosities of nanocomposite samples sintered for 1 h in argon

SiC content / wt%	Sintering temperature / °C	Theoretical density / ($g \cdot cm^{-3}$)	Bulk density / ($g \cdot cm^{-3}$)	Relative density / %	Apparent porosity / %
0	775	8.96	8.49	94.7	3.78
1		8.80	8.28	94.1	4.52
2		8.65	8.06	93.2	5.71
4		8.36	7.65	91.5	7.66
8		7.84	7.01	89.4	9.11
0	875	8.96	8.73	97.4	2.11
1		8.80	8.55	97.1	2.51
2		8.65	8.32	96.2	3.37
4		8.36	7.95	95.1	4.99
8		7.84	7.34	93.6	6.94

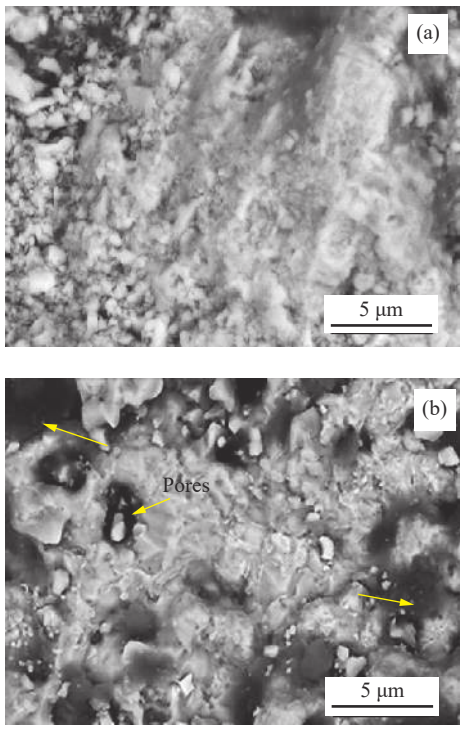

Fig. 7. SEM micrographs of the (a) Cu–2wt%SiC and (b) Cu–8wt%SiC specimens sintered at 775°C.

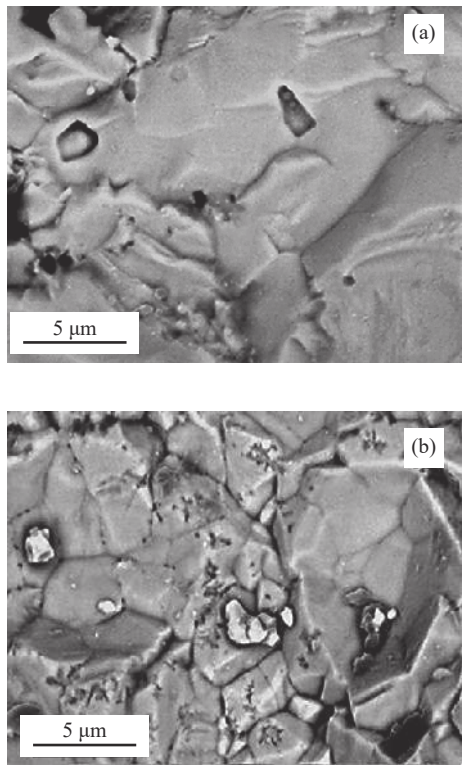

Fig. 8. SEM micrographs of the (a) Cu–2wt%SiC and (b) Cu–8wt%SiC specimens sintered at 875°C.

ature. The theoretical CTE values for Cu–0wt%, 1wt%, 2wt%, 4wt%, and 8wt% SiC nanocomposites calculated using the simple rule of mixtures were 17×10^{-6}, 16.64×10^{-6}, 16.28×10^{-6}, 15.61×10^{-6}, and 14.40×10^{-6} °C^{-1}, respectively. The CTE of unreinforced Cu sintered at 875°C was 15.67×10^{-6} °C^{-1} and the addition of 1wt%, 2wt%, 4wt%, and 8wt% SiC reduced the CTE values to 14.81×10^{-6}, 14.07×10^{-6}, 12.9×10^{-6}, and 11.1×10^{-6} °C^{-1}, respectively. Interestingly, the theoretical CTE values of the sintered samples were greater than the experimental values because of the high bonding between Cu matrix and SiC particles, which indicated the excellent interfacial bonding also imposes effective constraint to the expansion of the Cu matrix [10,37]. Generally, the lower CTE of the Cu matrix with the addition of SiC particles should be attributed to the lower CTE of SiC (3.7×10^{-6} °C^{-1}) than that of Cu matrix (17×10^{-6} °C^{-1}), which comes from the interfacial bonding between the SiC nanoparticles and Cu matrix. Furthermore, for nanocomposite samples, residual stresses (compression and tensile stresses) resulting from thermal mismatch between the Cu matrix and SiC particles play a strong role in determining the behavior of thermal expansion [36]. Alternatively, increasing the thermal expansion of nanocomposites with increased sintering temperature from 775 to 875°C is compatible with the relative density and apparent porosity because of the microstructure development and densification [38]. The thermal mismatch

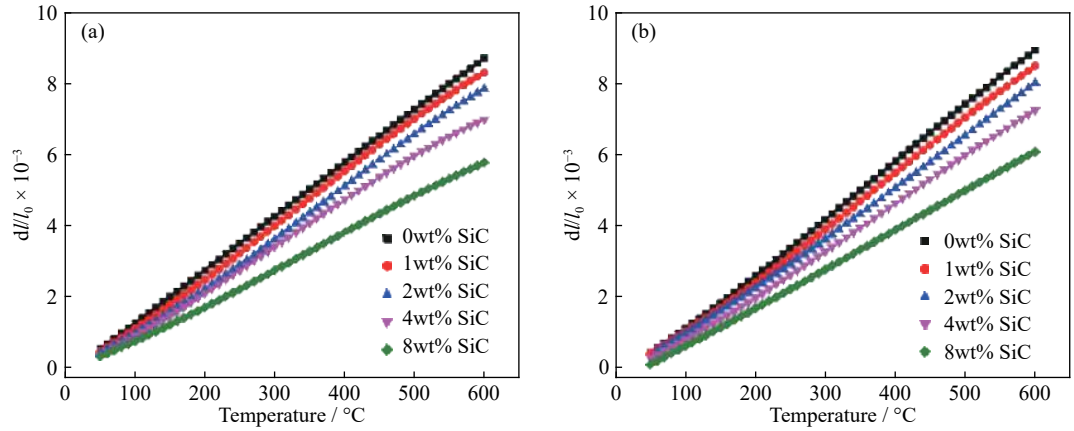

Fig. 9. Variations of the thermal expansion of nanocomposites sintered for 1 h at (a) 775°C and (b) 875°C.

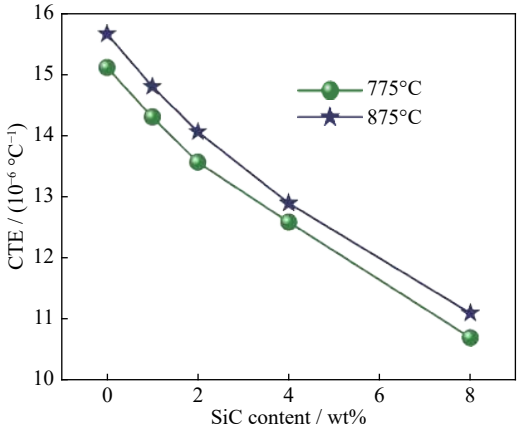

Fig. 10. Effects of SiC weight percentage and sintering temperature on CTE values of nanocomposites samples.

generates a residual stress field in the Cu matrix and SiC reinforcement where the pores undergo a compression stress that causes shrinkage of the pore volume. Subsequently, the thermal expansion and CTE value of the composite decrease with an increase in the porosity and vice versa [10].

An efficiency factor (i.e., F) is used to assess the influence of SiC content and sintering temperature on the CTE of the Cu matrix nanocomposite according to Eq. (12) [39]:

$$F = \frac{\alpha_c - \alpha_m}{V} \tag{12}$$

where α_c and α_m are the CTE values of the nanocomposite and Cu, respectively; V is the SiC volume percentage. The relationship between F and SiC content are represented in Fig. 11, where the F value decreased with increasing SiC content but increased with temperature.

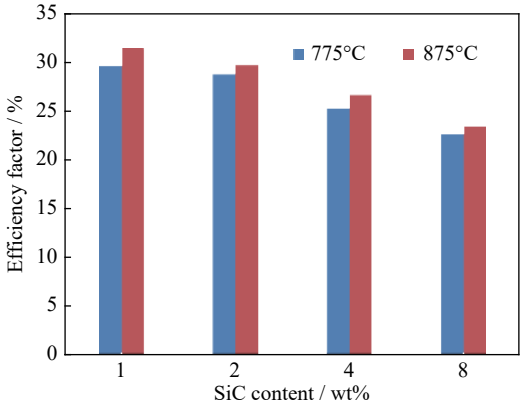

Fig. 11. Effects of weight percentage of SiC and sintering temperature on the *F* values of nanocomposite samples.

3.2.4. Mechanical properties

Fig. 12 shows the microhardness values of the Cu/SiC nanocomposite samples. The microhardness values of the nanocomposites were greater than that of the unreinforced Cu sample processed in the same sintering temperature. Furthermore, the microhardness increased with an increase in SiC

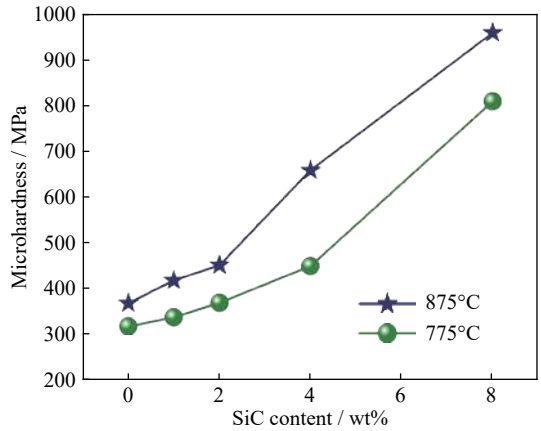

Fig. 12. Microhardness of the Cu/SiC nanocomposite specimens.

weight percentage and sintering temperature. The standard hardness values of Cu and SiC range from 343 to 369 MPa and 23.5 to 25.5 GPa, respectively. The microhardness increased and reached 808.9 MPa for the composite sample containing 8wt% SiC sintered at 775°C. With increasing sintering temperature up to 875°C, the microhardness further increased to 958.7 MPa for the composite sample. The longitudinal and shear ultrasonic velocities (i.e., V_L and V_S) are represented in Fig. 13, and the elastic moduli of the sintered samples are listed in Table 2. Notably, V_L and V_S increased with SiC weight percentage and sintering temperature. The results in Fig. 13 indicated that with an increase in SiC content from 0wt% to 8wt%, the V_L values of the samples sintered at 775 and 875°C increased from 4301 to 6202 m·s^{-1} and 4419 to 6514 m·s^{-1}, respectively, and the V_S values ranged from 2167 to 3082 m·s^{-1} and 2210 to 3214 m·s^{-1}, respectively. As a result, the elastic moduli had the same trend as the ultrasonic velocities (Table 2). The elastic modulus of the nanocomposite samples with 8wt% SiC sintered at 775 and 875°C (261.9 and 309.9 GPa, respectively) were greater than those of unreinforced Cu matrix sintered at the same temperatures (154.5 and 171.1 GPa, respectively).

Fig. 14 displays the room temperature (i.e., 30°C) compressive stress–strain curves for the Cu/SiC nanocomposites with different SiC contents and sintered at 775 and 875°C. The ultimate strength, yield strength, and elongation are listed in Fig. 15. The strength revealed significant improvement with the addition of nano-SiC particles and the increased sintering temperature. Moreover, the addition of SiC particles was responsible for a considerable decrease in the ductility of the Cu matrix while it increased with increased sintering temperature. The elongation was reduced from ~29.7% for Cu matrix to ~19.2% for the Cu with 8wt% SiC nanocomposite sintered at 775°C; however, when the sintered temperature was 875°C, the elongation was reduced from 33.7% to 21%. The apparent strengthening efficiency

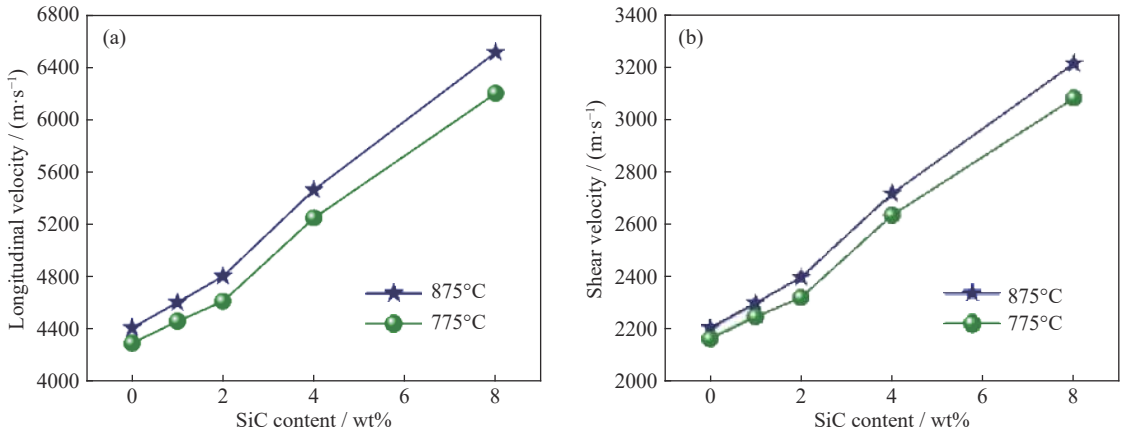

Fig. 13. (a) Longitudinal and (b) shear ultrasonic velocities of Cu/SiC nanocomposites at different sintering temperatures.

Table 2. Young's modulus (*E*), elastic modulus (*L*), bulk modulus (*K*), shear modulus (*G*), and Poisson's ratio (*v*) of nanocomposite samples sintered for 1 h in argon

SiC content / wt%	Sintering temperature / °C	*E* / GPa	*L* / GPa	*K* / GPa	*G* / GPa	*v*
0	775	104.3	154.5	39.2	39.2	0.3299
1		109.8	162.7	41.3	41.3	0.3301
2		113.1	167.8	42.5	42.5	0.3304
4		137.5	204.9	51.6	51.6	0.3316
8		172.9	261.9	64.7	64.7	0.3360
0	875	114.1	171.2	128.3	42.8	0.3332
1		121.4	182.4	136.9	45.5	0.3337
2		128.5	193.2	145.0	48.2	0.3340
4		157.3	237.9	179.0	58.9	0.3355
8		202.1	309.9	234.5	75.5	0.3391

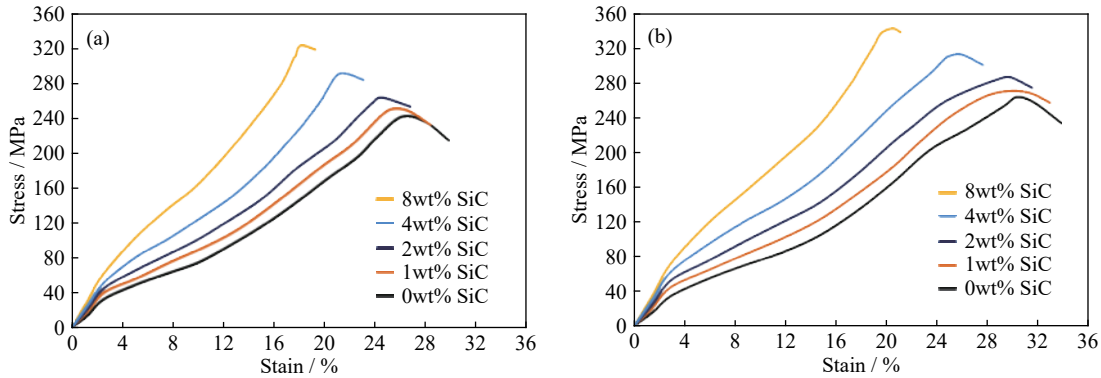

Fig. 14. Compressive curves of the nanocomposites sintered at (a) 775°C and (b) 875°C.

(i.e., R_a) of nanocomposites samples as a function of the SiC content is presented in Fig. 16. The improvement in R_a was a result of increasing both the SiC content and sintering temperature. The R_a value can be calculated as follows [40]:

$$R_a = \frac{\sigma_c - \sigma_m}{V\sigma_m} \tag{13}$$

where σ_c and σ_m are the yield strength of nanocomposite and Cu matrix, respectively; V is the volume fraction of the reinforcement particles. Based on these results, adding various weight percentages of nano-SiC to the Cu matrix remarkably improved the mechanical properties, including the Vickers microhardness, elastic moduli, ultimate strength, yield strength, and strengthening efficiency. These improvements may be a result of the addition of very hard SiC particles to the ductile Cu matrix, uniform distribution of nano-SiC particles, and grain refinement [41].

The addition of SiC particles to the Cu matrix also con-

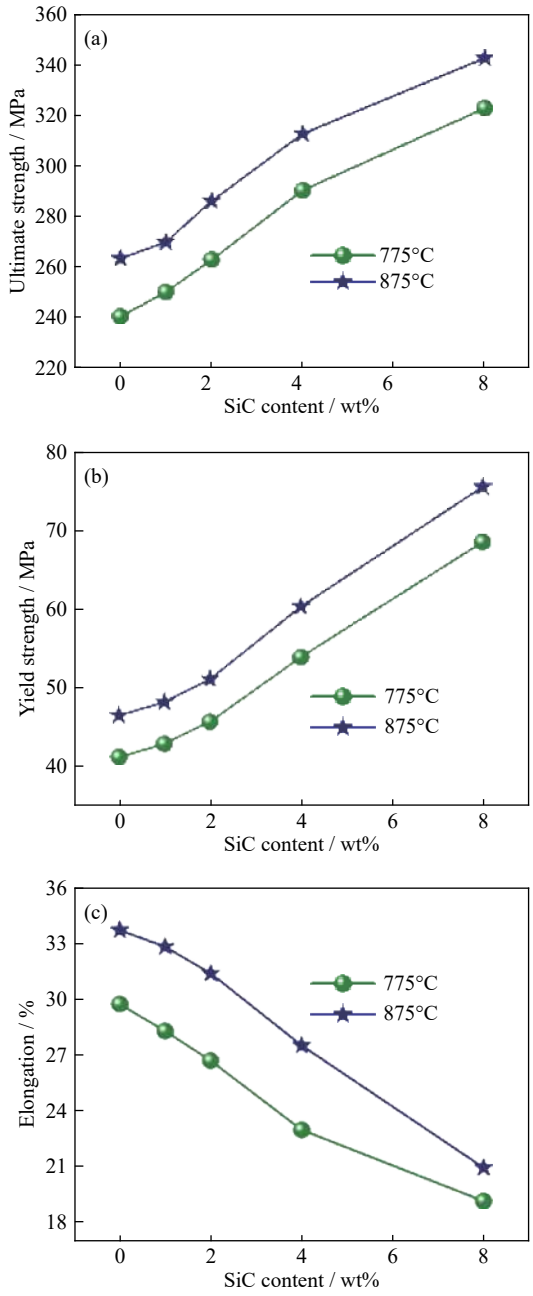

Fig. 15. (a) Ultimate strengths, (b) yield strengths, and (c) elongations of Cu/SiC nanocomposites samples.

tributes to transferring the applied load from the Cu matrix to SiC, which consequently increases the resistance to the plastic deformation of the sintered nanocomposite samples because of the variation in CTE value of the Cu matrix and SiC reinforcement particles. Accordingly, the thermal mismatch increases the dislocation density in the vicinity of SiC (Section 3.1.1), increasing the strength of the nanocomposite samples. The thermal stresses enhance the microhardness of the nanocomposites and flow stresses in the samples, making the plastic deformation more difficult [42]. Furthermore, the grain boundaries increase because of grain refinement that

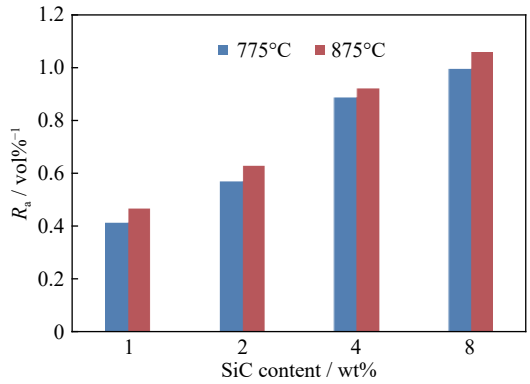

Fig. 16. Apparent strengthening efficiencies (R_a) of the nanocomposite specimens.

occurs after milling [43]. The interaction between the reinforcement and dislocations is a major reason for the strength of the composite materials. The "Orowan mechanism" describes that the passage of dislocations via particles introduces residual dislocation loops around each particle. Indeed, these particles act to enhance the strength of the material by prohibiting the migration of dislocations [5,44].

Alternatively, the decrease rate in ductility of the nanocomposite sample exhibits a considerable increase because of the successive addition of SiC particles. The main reason behind this reduction in ductility with the addition of SiC is the weak bonds between SiC and the Cu matrix, which act as stress concentrators and contribute to the formation of micro cracks, propagation, and fracture of the nanocomposite samples in compression [45]. In general, the enhancement in the mechanical properties with increasing sintering temperature from 775 to 875°C is closely correlated to the densification of the studied sample. The increasing sintering temperature causes a decrease in the inter-atomic spacing, which consequently increases the propagation of ultrasonic waves in the nanocomposites samples and therefore increases the value of the elastic moduli and acceleration of the diffusion process [46].

3.3. Electrical properties

The dependence of electrical conductivity of the sintered nanocomposites on SiC content, at two different sintering temperatures, is illustrated in Fig. 17. Notably, the electrical conductivity decreased with an increase in SiC particle content, while it increased with increasing sintering temperature. The conductivity of metal is highly dependent on the movement of electrons into the structure. However, the addition of SiC particles contributed to distorting this structure and hindering the movement of the Cu electrons, and accordingly, the conductivity was reduced [47]. After the milling process, the grain boundaries increased as a result of grain refinement, which prohibited the electron path. In addition, the dislocations and porosity increased as a result of the ceramic particles, leading to an electron scattering phenomenon

[3,48]. When increasing the sintering temperature, the conductivity of the nanocomposite samples increased as a result of the reduced porosity. Similar results were reported by Islak [49], Ayyappadas *et al*. [50], and Taha and Zawrah [4]. Moreover, Moustafa and Taha [2] reported that the electrical conductivity is directly proportional to the sintering temperature of the Cu matrix composites.

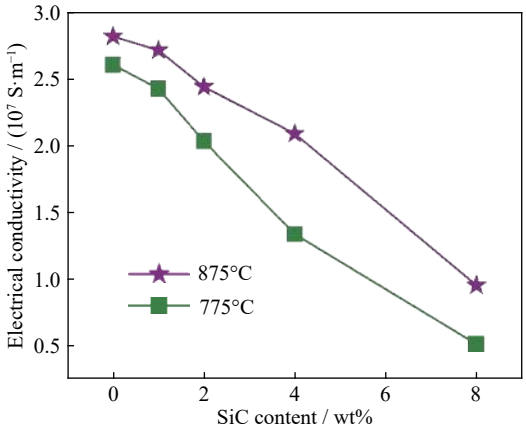

Fig. 17. Electrical conductivities of the nanocomposites at different sintering temperatures.

4. Conclusions

Cu matrix nanocomposites containing various contents of nano-SiC, i.e., 0wt%, 1wt%, 2wt%, 4wt%, and 8wt%, were successfully prepared by mechanical alloying via cold pressing and sintering for 1 h at 775 and 875°C in an argon atmosphere. The following conclusions were made:

(1) CTE, efficiency factor, and electrical conductivity values were reduced with the increased weight percentage of SiC particles, indicating high dimensional stability. Moreover, the values considerably increased with the increased sintering temperature.

(2) The microhardness and Young's modulus for the Cu–8wt%SiC sample sintered at 775°C in an argon atmosphere for 1 h were 808.9 MPa and 172.9 GPa, respectively. At the sintering temperature of 875°C, the microhardness and Young's modulus values of the same nanocomposite were 958.7 MPa and 202.1 GPa, respectively.

(3) Under compression testing, the ultimate and yield strengths of the samples sintered at 875°C increased from 263.7 MPa and 46.5 MPa to approximately 342.5 MPa and 75.5 MPa, respectively, with the content of additive SiC particles up to 8wt%, which were ~30% and ~62.4% increases.

Acknowledgements

This work was supported by the Deanship of Scientific Research (DSR), King Abdulaziz University, Jeddah, Saudi Arabia under grant No. (G: 30-135-1441). The authors therefore acknowledge with thanks DSR for the technical and financial support.

References

[1] S.L. Fu, X.H. Chen, and P. Liu, Preparation of CNTs/Cu composites with good electrical conductivity and excellent mechanical properties, *Mater. Sci. Eng. A*, 771(2020), art. No. 138656.

[2] E.B. Moustafa and M.A. Taha, Preparation of high strength graphene reinforced Cu-based nanocomposites via mechanical alloying method: Microstructural, mechanical and electrical properties, *Appl. Phys. A*, 126(2020), No. 3, art. No. 220.

[3] Y.A. Sorkhe, H. Aghajani, and A.T. Tabrizi, Mechanical alloying and sintering of nanostructured TiO_2 reinforced copper composite and its characterization, *Mater. Des.*, 58(2014), p. 168.

[4] M.A. Taha and M.F. Zawrah, Effect of nano ZrO_2 on strengthening and electrical properties of Cu-matrix nanocomposits prepared by mechanical alloying, *Ceram. Int.*, 43(2017), No. 15, p. 12698.

[5] M.R. Akbarpour, H.M. Mirabad, and S. Alipour, Microstructural and mechanical characteristics of hybrid SiC/Cu composites with nano- and micro-sized SiC particles, *Ceram. Int.*, 45(2019), No. 3, p. 3276.

[6] M.F. Zawrah, H.A. Mostafa, and M.A. Taha, Effect of SiC content on microstructure, mechanical and electrical properties of sintered Al–20Si–*x*SiC nanocomposites fabricated by mechanical alloying, *Mater. Res. Express*, 6(2019), No. 12, art. No. 125014.

[7] J.R. Yang, L. Wang, X.R. Tan, Q. Zhi, R.B. Yang, G.P. Zhang, Z.X. Liu, X.H. Ge, and E.J. Liang, Effect of sintering temperature on the thermal expansion behavior of $ZrMgMo_3O_{12p}$/2024Al composite, *Ceram. Int.*, 44(2018), No. 9, p. 10744.

[8] A.Z. Naser and B.M. Darras, Experimental investigation of Mg/SiC composite fabrication via friction stir processing, *Int. J. Adv. Manuf. Technol.*, 91(2017), p. 781.

[9] M.A. Taha, A.H. Nassar, and M.F. Zawrah, *In-situ* formation of composite having hard outer layer based on aluminum dross reinforced by SiC and TiO_2, *Constr. Build. Mater.*, 248(2020), art. No. 118638.

[10] M.N. Arif, M.Z. Bukhari, D. Brabazon, and M.S.J. Hashmi, Coefficient of thermal expansion (CTE) study in metal matrix composite of CuSiC vs AlSiC, *IOP Conf. Ser.*: *Mater. Sci. Eng.*, 701(2019), No. 1, art. No. 012057.

[11] J. Sheng, L.D. Wang, D. Li, W.P. Cao, Y. Feng, M. Wang, Z.Y. Yang, Y. Zhao, and W.D. Fei, Thermal expansion behavior of copper matrix composite containing negative thermal expansion $PbTiO_3$ particles, *Mater. Des.*, 132(2017), p. 442.

[12] J. Khosravi, M.K.B. Givi, M. Barmouz, and A. Rahi, Microstructural, mechanical, and thermophysical characterization of Cu/WC composite layers fabricated via friction stir processing, *Int. J. Adv. Manuf. Technol.*, 74(2014), p. 1087.

[13] C.J. Hsu, C.Y. Chang, P.W. Kao, N.J. Ho, and C.P. Chang, Al–Al_3Ti nanocomposites produced *in situ* by friction stir processing, *Acta Mater.*, 54(2006), No. 19, p. 5241.

[14] M.A. Taha, A.H. Nassar, and M.F. Zawrah, Improvement of wettability, sinterability, mechanical and electrical properties of Al_2O_3–Ni nanocomposites prepared by mechanical alloying,

Ceram. Int., 43(2017), No. 4, p. 3576.
[15] R.A. Youness, M.A. Taha, and M.A. Ibrahim, Effect of sintering temperatures on the *in vitro* bioactivity, molecular structure and mechanical properties of titanium/carbonated hydroxyapatite nanobiocomposites, *J. Mol. Struct.*, 1150(2017), p. 188.
[16] M.A. Taha, R.A. Youness, and M. Ibrahim, Biocompatibility, physico-chemical and mechanical properties of hydroxyapatite-based silicon dioxide nanocomposites for biomedical applications, *Ceram. Int.*, 46(2020), No. 15, p. 23599.
[17] R.A. Youness, M.A. Taha, and M.A. Ibrahim, *In vitro* bioactivity, molecular structure and mechanical properties of zirconia-carbonated hydroxyapatite nanobiocomposites sintered at different temperatures, *Mater. Chem. Phys.*, 239(2020), art. No. 122011.
[18] M.A. Taha, R.A. Youness, and M.F. Zawrah, Review on nanocomposites fabricated by mechanical alloying, *Int. J. Miner. Metall. Mater.*, 26(2019), No. 9, p. 1047.
[19] R.A. Youness, M.A. Taha, and M. Ibrahim, Dense alumina-based carbonated fluorapatite nanobiocomposites for dental applications, *Mater. Chem. Phys.*, 257(2021), art. No. 123264.
[20] R.A. Youness, M.A. Taha, H. Elhaes, and M. Ibrahim, Molecular modeling, FTIR spectral characterization and mechanical properties of carbonated-hydroxyapatite prepared by mechanochemical synthesis, *Mater. Chem. Phys.*, 190(2017), p. 209.
[21] R.A. Youness, M.A. Taha, H. Elhaes, and M. Ibrahim, Preparation, fourier transform infrared characterization and mechanical properties of hydroxyapatite nanopowders, *J. Comput. Theor. Nanosci.*, 14(2017), No. 5, p. 2409.
[22] R.A. Youness, M.A. Taha, A.A. El-Kheshen, N. El-Faramawy, and M. Ibrahim, *In vitro* bioactivity evaluation, antimicrobial behavior and mechanical properties of cerium-containing phosphate glasses, *Mater. Res. Express*, 6(2019), No. 7, art. No. 075212.
[23] R.A. Youness, M.A. Taha, A.A. El-Kheshen, and M. Ibrahim, Influence of the addition of carbonated hydroxyapatite and selenium dioxide on mechanical properties and *in vitro* bioactivity of borosilicate inert glass, *Ceram. Int.*, 44(2018), No. 17, p. 20677.
[24] M.A. Ouis, M.A. Taha, G.T. El-Bassyouni, and M.A. Azooz, Thermal, mechanical and electrical properties of lithium phosphate glasses doped with copper oxide, *Bull. Mater. Sci.*, 42(2019), art. No. 246.
[25] M.F. Zawrah, M.A. Taha, and H.A. Mostafa, *In-situ* formation of Al_2O_3/Al core-shell from waste material: Production of porous composite improved by graphene, *Ceram. Int.*, 44(2018), No. 9, p. 10693.
[26] M. Hu, Y.L. Zhang, L.L. Tang, L. Shan, J. Gao, and P.L. Ding, Surface modifying of SiC particles and performance analysis of SiC_p/Cu composites, *Appl. Surf. Sci.*, 332(2015), p. 720.
[27] M.A. Taha, G.M. Elkomy, H.A. Mostafa, and E.S. Gouda, Effect of ZrO_2 contents and ageing times on mechanical and electrical properties of Al–4.5wt.% Cu nanocomposites prepared by mechanical alloying, *Mater. Chem. Phys.*, 206(2018), p. 116.
[28] M.A. Taha and M.F. Zawrah, Mechanical alloying and sintering of a Ni/10wt.%Al_2O_3 nanocomposite and its characterization, *Silicon*, 10(2018), p. 1351.
[29] D. Ağaoğulları, Effects of ZrC content and mechanical alloying on the microstructural and mechanical properties of hypoeutectic Al–7wt.% Si composites prepared by spark plasma sintering, *Ceram. Int.*, 45(2019), No. 10, p. 13257.
[30] A.S. Prosviryakov, SiC content effect on the properties of Cu–SiC composites produced by mechanical alloying, *J. Alloys Compd.*, 632(2015), p. 707.
[31] M. Karadag and G. Acikbas, Investigation of electrical and mechanical properties of Cu matrix TiC reinforced composites, *Sch. J. Eng. Technol.*, 6(2018), No. 2, p. 58.
[32] Y. Sahin and M. Acılar, Production and properties of SiCp-reinforced aluminium alloy composites, *Composites Part A*, 34(2003), No. 8, p. 709.
[33] W.S. AbuShanab, E.B. Moustafa, M.A. Taha, and R.A. Youness, Synthesis and structural properties characterization of titania/zirconia/calcium silicate nanocomposites for biomedical applications, *Appl. Phys. A*, 126(2020), No. 10, art. No. 787.
[34] R.A. Youness, M.A. Taha, and M. Ibrahim, *In vitro* bioactivity, physical and mechanical properties of carbonated-fluoroapatite during mechanochemical synthesis, *Ceram. Int.*, 44(2018), No. 17, p. 21323.
[35] M. Rahimian, N. Ehsani, N. Parvin, and H. reza Baharvandi, The effect of particle size, sintering temperature and sintering time on the properties of Al–Al_2O_3 composites, made by powder metallurgy, *J. Mater. Process. Technol.*, 209(2009), No. 14, p. 5387.
[36] Z.B. Lei, K. Zhao, Y.G. Wang, and L.N. An, Thermal expansion of Al matrix composites reinforced with hybrid micro-/nano-sized Al_2O_3 particles, *J. Mater. Sci. Technol.*, 30(2014), No. 1, p. 61.
[37] K. Azmi, M.N. Derman, and A.M.M.A. Bakri, The themal expansion behavior of Cu–SiC_p composites, *Adv. Mater. Res.*, 795(2013), p. 237.
[38] W.F. Guo, Y.Z. Wang, A.D. Li, T.F. Jiao, and F.M. Gao, Effect of sintering temperature on microstructure, electrical properties, and thermal expansion of perovskite-type $La_{0.8}Ca_{0.2}CrO_3$ complex oxides synthesized by a combustion method, *J. Electron. Mater.*, 42(2013), No. 6, p. 939.
[39] W.S. AbuShanab, E.B. Moustafa, E. Ghandourah, and M.A. Taha, Effect of graphene nanoparticles on the physical and mechanical properties of the Al2024-graphene nanocomposites fabricated by powder metallurgy, *Results Phys.*, 19(2020), art. No. 103343.
[40] L.D. Wang, Y. Cui, B. Li, S. Yang, R.Y. Li, Z. Liu, R. Vajtai, and W.D. Fei, High apparent strengthening efficiency for reduced graphene oxide in copper matrix composites produced by molecule-lever mixing and high-shear mixing, *RSC Adv.*, 5(2015), No. 63, p. 51193.
[41] C. Carreño-Gallardo, I. Estrada-Guel, C. López-Meléndez, E. Ledezma-Sillas, R. Castañeda-Balderas, R. Pérez-Bustamante, and J.M. Herrera-Ramírez, B_4C particles reinforced Al2024 composites via mechanical milling, *Metals*, 8(2018), No. 8, p. 647.
[42] P.R. Matli, F. Ubaid, R.A. Shakoor, G. Parande, V. Manakari, M. Yusuf, A.M.A. Mohamed, and M. Gupta, Improved properties of Al–Si_3N_4 nanocomposites fabricated through a microwave sintering and hot extrusion process, *RSC Adv.*, 7(2017), No. 55, p. 34401.
[43] F.Y. Chen, J.M. Ying, Y.F. Wang, S.Y. Du, Z.P. Liu, and Q. Huang, Effects of graphene content on the microstructure and properties of copper matrix composites, *Carbon*, 96(2016), p. 836.
[44] M.A. Taha, R.A. Youness, and M.A. Ibrahim, Evolution of the physical, mechanical and electrical properties of sic-reinforced Al 6061 composites prepared by stir cast method, *Biointerface Res. Appl. Chem.*, 11(2021), No. 2, p. 8946.
[45] E. Tekoğlu, D. Ağaoğulları, Y. Yürektürk, B. Bulut, and M.L. Öveçoğlu, Characterization of LaB_6 particulate-reinforced eutectic Al–12.6wt% Si composites fabricated via mechanical alloying and spark plasma sintering, *Powder Technol.*, 340(2018),

p. 473.
[46] C.D. Wu, P. Fang, G.Q. Luo, F. Chen, Q. Shen, L.M. Zhang, and E.J. Lavernia, Effect of plasma activated sintering parameters on microstructure and mechanical properties of Al-7075/B_4C composites, *J. Alloys Compd.*, 615(2014), p. 276.
[47] G.C. Efe, M. Ipek, S. Zeytin, and C. Bindal, An investigation of the effect of SiC particle size on Cu–SiC composites, *Composites Part B*, 43(2012), No. 4, p. 1813.
[48] D.-H. Kwon, D.N. Thuy, X.H. Khoa, P.-P. Choi, M.-G. Chang, Y.-J. Yum, J.S. Kim, and Y.S. Kwon, Mechanical, electrical and wear properties of Cu–TiB_2 nanocomposites fabricated by MA-SHS and SPS, *J. Ceram. Process. Res.*, 7(2006), No. 3, p. 275.
[49] S. Islak, D. Kır, and S. Buytoz, Effect of sintering temperature on electrical and microstructure properties of hot pressed Cu–TiC composites, *Sci. Sintering*, 46(2014), No. 1, p. 15.
[50] C. Ayyappadas, A. Muthuchamy, A.R. Annamalai, and D.K. Agrawal, An investigation on the effect of sintering mode on various properties of copper–graphene metal matrix composite, *Adv. Powder Technol.*, 28(2017), No. 7, p. 1760.